JOURNAL OF MATERIALS SCIENCE 28 (1993) 6285–6294

Effects of oxidation of Cr_3C_2 particulate-reinforced alumina composites on microstructure and mechanical properties

CHEN-TSU FU*, AI-KANG LI, JENN-MING WU*
*Material Research Laboratories Industrial Technology Research Institute, and * Department of Materials Science and Engineering National Tsing Hua University, Hsinchu 31015, Taiwan*

Al_2O_3 can be strengthened and toughened by incorporating Cr_3C_2 particles through hot-pressing. For instance, an Al_2O_3–10 vol% Cr_3C_2 composite exhibits fracture strength and toughness of 600 MPa and 5.5 Mpa $m^{0.5}$, respectively. An annealing treatment in air from 1000–1200 °C may further substantially strengthen the same composite to give $\sigma_f = 800$ MPa and $K_{IC} = 9.5$ MPa $m^{0.5}$. Possible oxidation reactions and toughening mechanisms are discussed in terms of oxygen diffusion, the formation of micropores beneath the exposed surface, as well as the fracture mode.

1. Introduction

Ceramic composites have attracted much attention because of their better mechanical properties, especially fracture toughness, which they possess either at room temperature or at elevated temperatures.

Most reinforcements used in ceramic composites are metal carbides, basically in an attempt to utilize their high-modulus characteristics. In an air environment, however, metal carbides are not thermodynamically stable and always have a tendency to convert to oxides. This phenomenon is very obvious when the temperature is high. Therefore, it is necessary to understand the oxidation behaviour of ceramic composites at elevated temperatures before they can practically be used.

Most oxidation studies reported in the literature for structural ceramics concentrated on monolithic non-oxides, such as SiC [1, 2] and Si_3N_4 [3, 4] to name but a few. Some results have demonstrated that oxidation treatments for the non-oxides not only can be used to improve fracture strength and toughness [1] but also to improve the relibility of the non-oxide ceramics [4]. In the past few years, some oxidation work has been performed on the oxide matrix composites containing carbide particulates or whiskers [5–9]. Owing to the chemical reactions between the composite constituents, the mechanical properties of these ceramic composites were degraded rather than upgraded after annealing in air. For instance, annealing of Al_2O_3/SiC composites will end up with alumina, mullite and non-equilibrium aluminosilicate glass as products and the flexural strength drastically declines.

Recently, we found [10, 11] that Cr_3C_2 particle-reinforced Al_2O_3 shows a significant improvement in the fracture toughness. At the same time, electrical resistivity of the composite is much lowered which makes electrical discharge machining (EDM) of this material possible. Further study of its oxidation behaviour seems quite natural after observing such encouraging properties. This paper reports the preliminary findings of the oxidation of Cr_3C_2 particles and its influence on the mechanical properties of the Al_2O_3/Cr_3C_2 composites.

2. Experimental procedure

2.1. Raw materials

The Cr_3C_2 particle used in this investigation was Herman C. Stark's product with particle size of 2–3 μm and a purity higher than 99%. The Al_2O_3 powder was Alcoa's (A16-SG) product, with particle size 0.3–0.5 μm and purity higher than 99.7%.

2.2. Consolidation procedures

First, Cr_3C_2 and Al_2O_3 powders were added together with deionized water and then ball-milled for 24 h. The slurry was further homogenized for 15 min using a high-shear ultrasonic dispersing process. The homogenized slurry was dried rapidly with constant agitation on a hot plate. The dried and sieved mixture was uniaxially pre-pressed to form discs with 5 mm high and 60 mm diameter. The green compacts were then placed in a boron nitride-coated graphite mould and hot-pressed at 1400 °C in an argon atmosphere, under a pressure of 30 MPa for 1 h.

2.3. Characterization

The dense composite discs were ground and cut, along the grinding direction, to $3 \times 4 \times 40$ mm bars. All specimens were polished with diamond pastes from 15 μm down to 3 μm. Each bar to be used for fracture toughness test, was centre-notched to one-third of its thickness using a 0.15 mm thick diamond blade. The oxidation treatments were performed by heating spe-

0022–2461

cimens in air at 1000 or 1200 °C for varying periods from 20–150 h. The flexural strength was measured through a four-point bending test following the JIS 1601 method and the fracture toughness was evaluated using the single-edge-notched beam (SENB) method [12]. Both of them were measured at room temperature. The microstructures of fracture surface and the exposed surface of the specimens were examined by scanning and transmission electron microscopy (SEM and TEM). The X-ray diffraction pattern was used to verify the chemical reactions between Cr_3C_2, Al_2O_3 and oxygen. The weight change of the specimens before and after the oxidation process was determined using a microbalance.

3. Results and discussion

3.1. Mechanical properties

Cr_3C_2 particulate-reinforced Al_2O_3 composites can be hot-pressed to greater than 98.5% theoretical density at 1400 °C, giving a flexural strength higher than 600 MPa. The sintering behaviour and mechanical properties of the Cr_3C_2/Al_2O_3 composites were presented elsewhere [10, 11].

Recent experiments have shown that annealing in air may induce a substantial increase of the mechanical properties of these composites. The relations between exposure time and fracture strength of 10 and 30 vol % Cr_3C_2/Al_2O_3 composites are shown in Fig. 1. For comparison, the flexural strength of alumina, 320 MPa, is plotted on the graph. All of the specimens of Cr_3C_2/Al_2O_3 composites show improved fracture strength after exposure at 1000 °C for 20–150 h. These results are completely different from the prior investigations [5, 6] in which the fracture strength of the ceramic composites being studied, degraded after having been oxidized at high temperatures. In this study, the increase of fracture strength is proportional to the oxidation time up to 100 h. At that time, the fracture strength of 10 vol % Cr_3C_2/Al_2O_3 composites reaches its maximum value of 805 MPa and then drops to 720 MPa as the exposure time is extended to 150 h. However this value is still greater than that of as-sintered composites (605 MPa). When the annealing temperature was raised from 1000 °C to 1200 °C, the strengthening effect was greatly reduced.

The microstructures observed from specimens taken before and after oxidation are shown in Fig. 2. Fig. 2a is a typical microstructure of unoxidized composites with Cr_3C_2 particles (white particles in the micrograph), uniformly distributed in the Al_2O_3 matrix. After oxidation, many micropores, which are located just beneath the exposed surface of the composite, are formed as shown in Fig. 2b. The pore shape is relatively nodular and the size, as directly measured from the micrograph, is about 5 μm. This value is truly reflected in the diameter of Cr_3C_2 particles in the sintered body. The critical flaw size for pure Al_2O_3 to have catastrophic failure may be calculated using the Griffith law, is 38 μm if a flexural strength of 320 MPa is chosen. Therefore, these pores forming from the oxidation of Cr_3C_2 particles are much smaller than the critical flaw size and will not have an adverse effect

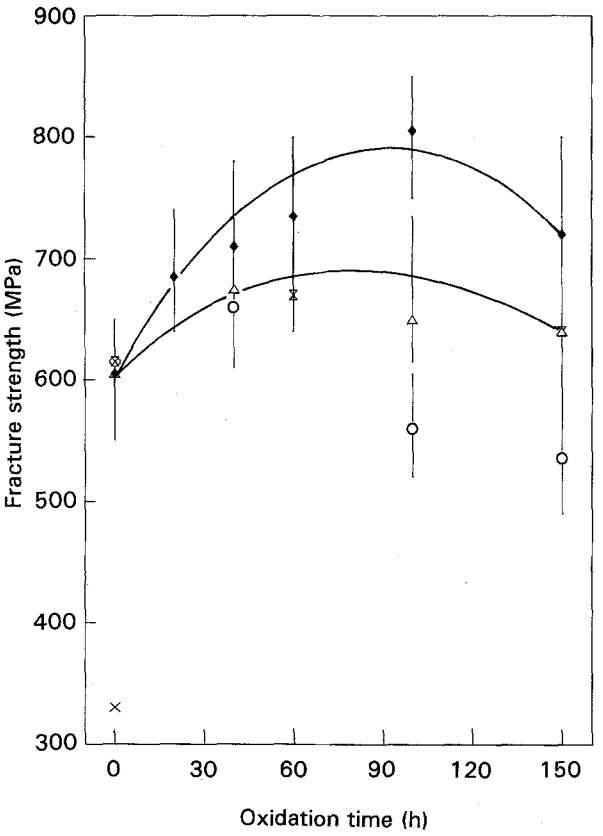

Figure 1 Room-temperature fracture strength of (◆, △) 10 and (⧖, ◯) 30 vol % Cr_3C_2 particulate-reinforced Al_2O_3 composites after oxidation at (◆, ⧖) 1000 and (△, ◯) 1200 °C. (×) Al_2O_3.

on the fracture strength. In Luthra's investigations [9, 13], many larger pores, in the 50 μm range, were observed beneath the exposed surface in the oxidized specimens of SiC-reinforced Al_2O_3 matrix composites. Thus the strength degradation originated from the larger flaws arising from the chemical reactions between carbide and oxygen. When more Cr_3C_2 was added to the composites, greater porosity was formed during the oxidation process and may deteriorate the stiffness of composites and cause degradation of strength. It can be observed that the 30 vol % Cr_3C_2 composite gives lower fracture strength than that of the 10 vol % Cr_3C_2 composite after an annealing treatment. The time dependence of annealing on the toughness change can also illustrate the role of micropores. The fracture toughness of composites as a function of exposure time at constant temperature (1000 °C) is shown in Fig. 3. For composites containing 10 vol % Cr_3C_2, the fracture toughness remarkably increases from 5.5 MPa $m^{0.5}$ to 9.3 MPa $m^{0.5}$ for more than 40 h exposure, while for the composites containing 30 vol % Cr_3C_2 the toughness remains almost at the same value as the untreated one, 8.0 MPa $m^{0.5}$.

The fractography of the specimens fractured at room temperature after oxidation is shown in Fig. 4. The fracture surface observed at different magnifications is shown in Fig. 4a and b. There are many spherical micropores and secondary cracks just located beneath the exposed surface. It is reasonable to say that crack blunting, which causes more energy

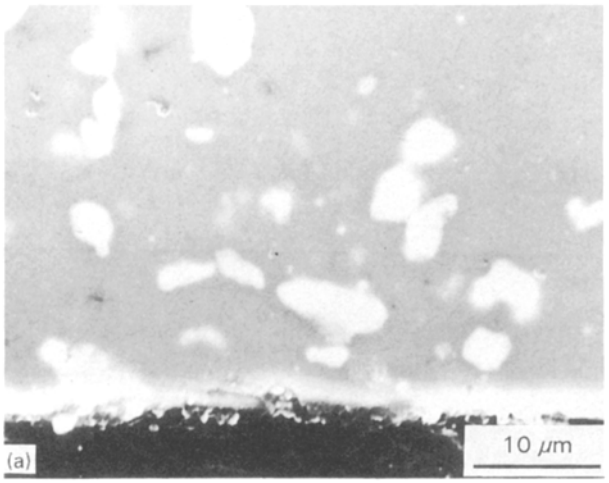

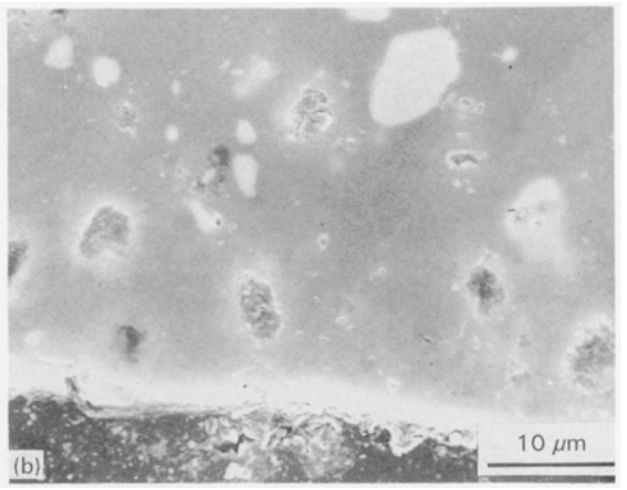

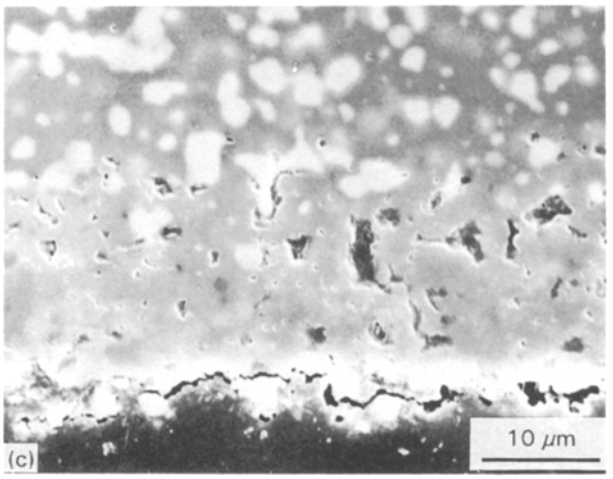

Figure 2 Cross-sectional scanning electron micrographs of Cr_3C_2/Al_2O_3 composites. (a) 10 vol % Cr_3C_2/Al_2O_3 composite, as sintered. (b) 10 vol % Cr_3C_2/Al_2O_3 composite after oxidation at 1200 °C for 40 h. (c) 30 vol % Cr_3C_2/Al_2O_3 composite after oxidation at 1200 °C for 40 h.

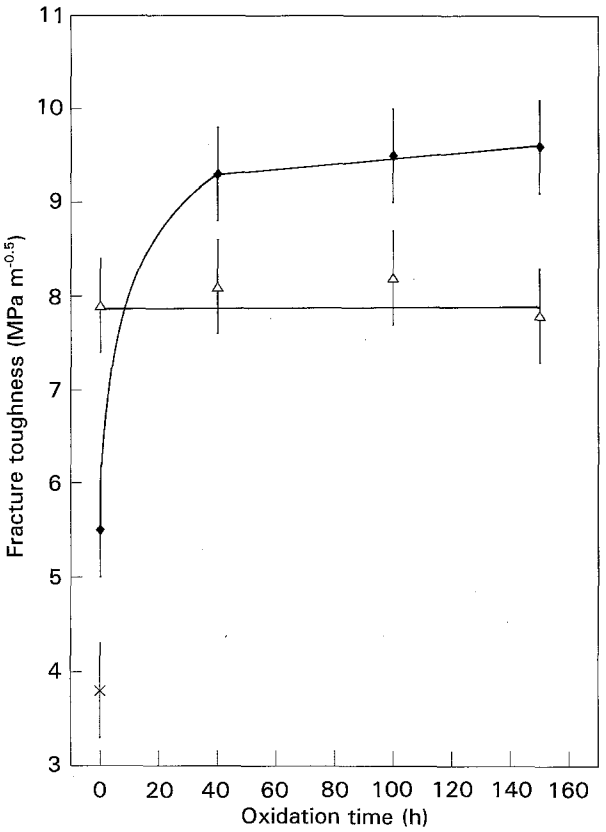

Figure 3 Fracture toughness of (◆) 10 and (△) 30 vol % Cr_3C_2-reinforced Al_2O_3 composites after oxidation at 1000 °C. (×) Al_2O_3.

dissipation, is the primary toughening mechanism. Fig. 4c shows the fracture surface of the unoxidized regions, indicating that the toughening mechanism of the internal portion is still based on the crack deflections and bridgings caused by the Cr_3C_2 particles.

The cross-sectional micrographs of secondary cracks in composites specimens after oxidation are shown in Fig. 5. The secondary cracks initiate from the micropores existing in oxidized surface, as shown in Fig. 5a. Those micropores will enhance the initiation of secondary cracks, thus increasing the total work of fracture. As the secondary cracks propagate inwards to the unoxidized regions and encounter the Cr_3C_2 particles, they will again propagate along Cr_3C_2/Al_2O_3 interfaces, as shown in Fig. 5b.

The schematic interaction between micropores or particles with cracks is shown in Fig. 6. Fig. 6a shows that Cr_3C_2 particles can effectively deflect the crack, while Fig. 6b shows the micropores beneath the exposed surface can act as crack-nucleation sites for secondary cracks, blunting the crack front and pinning the crack. As the pores are incorporated, however, the reduction in new surface which the propagating crack must create is an adverse effect on the toughness of the materials. So the net effect of pores on the toughness for the ceramic material depends on the contents and geometrical morphology of the pores in the ceramics. This is the reason why the fracture toughness of composites containing 10 vol % Cr_3C_2 increases with oxidation time, but the composites containing 30 vol % Cr_3C_2 are independent of oxidation time.

3.2. Characterization of product phase and weight change

X-ray diffraction patterns taken from the exposed surface of composites are shown in Fig. 7. The Cr_2O_3

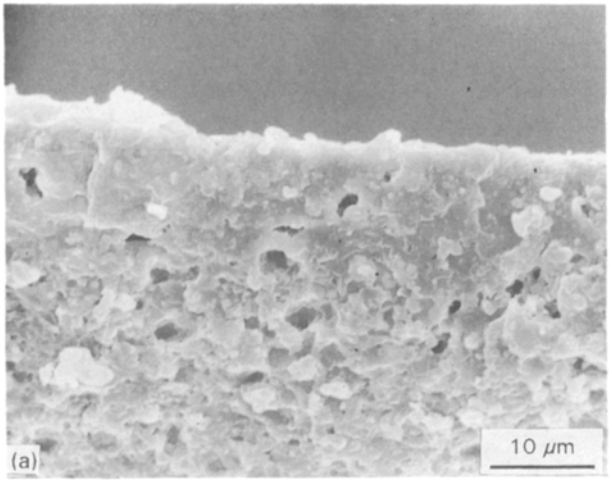

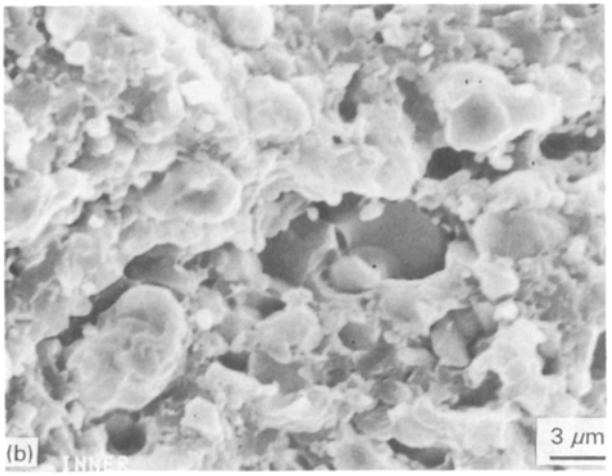

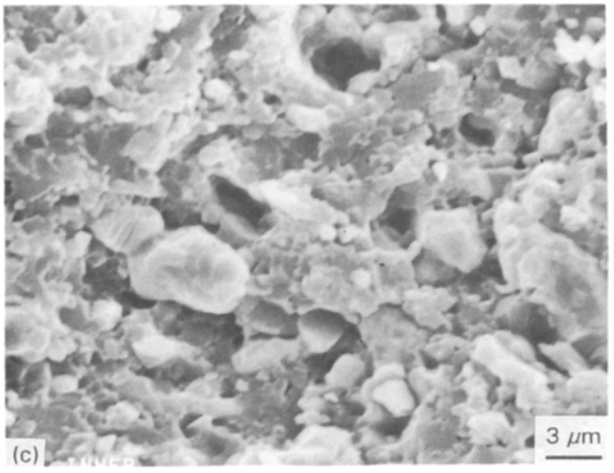

Figure 4 Scanning electron micrographs of the fracture surface of 30 vol % Cr_3C_2-reinforced Al_2O_3 composites after oxidation at 1200 °C, for 100 h. (a) Lower magnification, beneath the exposed surface. (b) Higher magnification of (a). (c) Fracture surface in the unoxidized region.

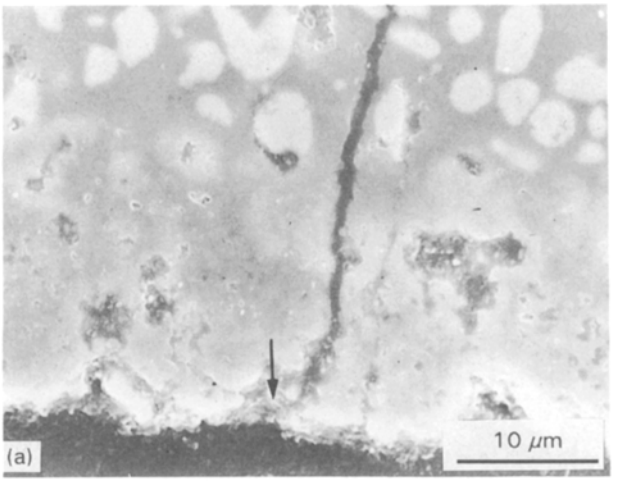

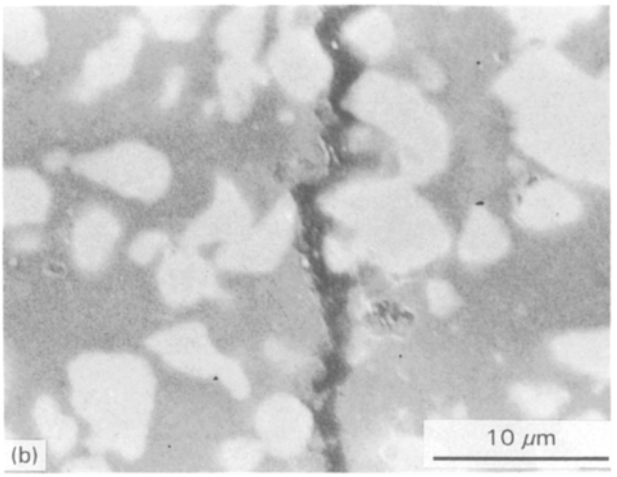

Figure 5 Cross-sectional scanning electron micrographs of Cr_3C_2-reinforced Al_2O_3 composites after oxidation, fracturing and polishing treatments: (a) the oxidized layer; the arrow indicates the microcrack will initiate at the location of micropores; (b) the unoxidized regions.

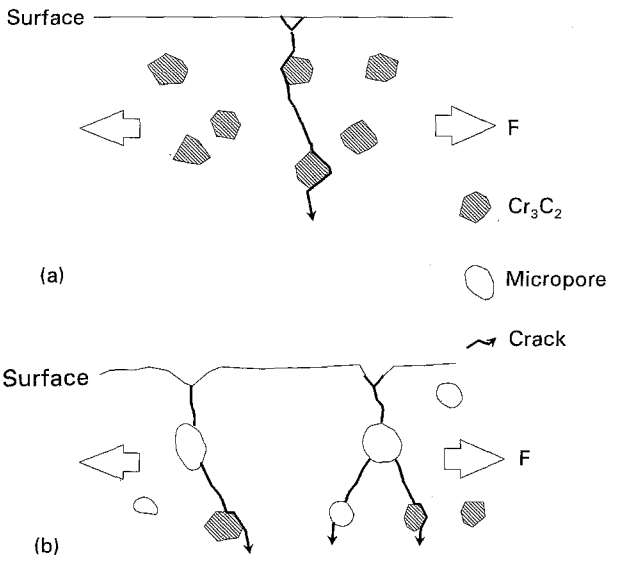

Figure 6 Schematic diagram illustrating the interactions between microcracks; micropores and Cr_3C_2 particles. (a) As-sintered composite, (b) after oxidation.

peaks were observed in all samples, indicating that the oxidation of Cr_3C_2 occurs by chemical Reaction 1, at least on the surface when the Al_2O_3/Cr_3C_2 composites were annealed in air. The Cr_2O_3 constituent phase is not a stable phase, as well proved in previous investigations [16, 17] when the temperature is greater than 1000 °C in dry air. Thus the Cr_2O_3 will continue to react with oxygen gas to form CrO_3 gaseous phase

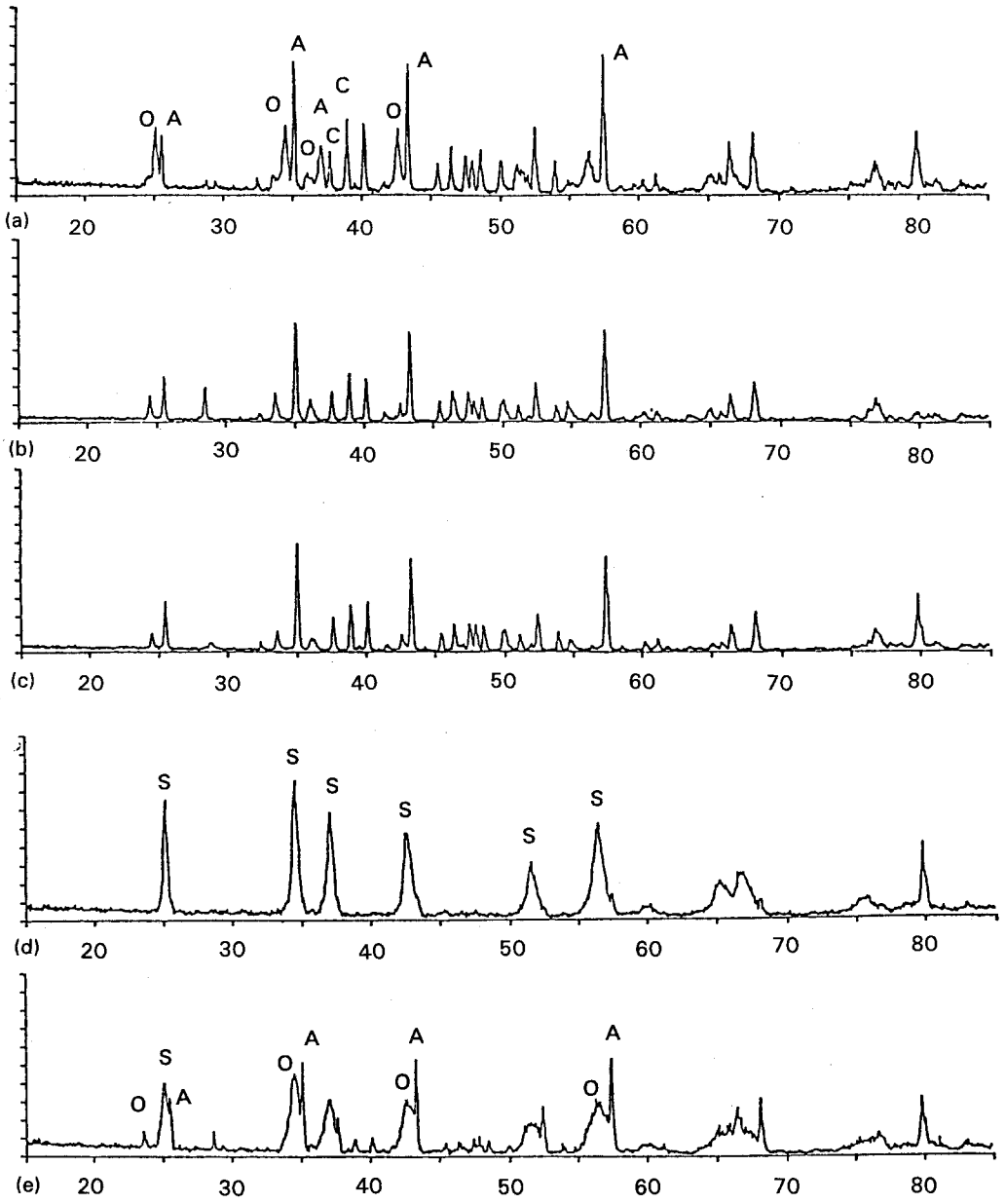

Figure 7 X-ray diffraction patterns of the oxidized surface: 30 vol % Cr_3C_2/Al_2O_3 composites after oxidation at 1000 °C for (a) 40 h, (b) 100 h, and (c) 150 h; 10 vol % Cr_3C_2/Al_2O_3 composites after oxidation at 1200 °C for (d) 40 h, and (e) 100 h. A, Al_2O_3; O, Cr_2O_3, C, Cr_3C_2; S, $Cr_2O_3 + Al_2O_3$.

in chemical Reaction 2. Because the CrO_3 is gaseous phase, it is very difficult to detect by XRD, the test results are shown in Fig. 7. But the possibility of Reaction 2 has been well proved in the published literature [16, 17].

$$2Cr_3C_{2(s)} + \frac{13}{2}O_{2(g)} = 3Cr_2O_{3(s)} + 4CO_{(g)} \quad (1)$$

$$Cr_2O_{3(s)} + \frac{3}{2}O_{2(g)} = 2CrO_{3(g)} \quad (2)$$

The chemical Reaction 2 is a reversible reaction. At elevated temperature CrO_3 gas will be vaporized out to form an atmosphere around the testing specimens. As the temperature is lowered, the CrO_3 vapour condenses and precipitates on the sample surface.

The peak intensity of Cr_2O_3 shown in Fig. 7a–c gradually drops with increasing oxidation time, illustrating that CrO_3 gas phase gradually evaporated out with oxidation time. When the oxidation temperature rises to 1200 °C, Cr_2O_3 particles will react with the Al_2O_3 matrix to form Al_2O_3–Cr_2O_3 solid solution. So the Cr_2O_3 and Al_2O_3 two peaks merged to a solid-solution broadening peak as shown in Fig. 7d. When the oxidation time increases from 40 h to 100 h, the Cr_2O_3–Al_2O_3 solid-solution peak gradually splits into Cr_2O_3 and Al_2O_3 two independent peaks again shown in Fig. 7e. These results suggest that Cr_2O_3 dissolves in Al_2O_3 matrix prior to vaporizing of Cr^{3+} on the surface of the sample.

Fig. 8 shows the correlations between weight change and oxidation time at 1000 and 1200 °C. The weight changes from a weight gain to a weight loss when the oxidation time increases from less than to more than 50 h at 1000 °C oxidation. The trends of weight change for both composites with 10 and

30 vol % content Cr_3C_2 are similar. But the rate of weight loss for 30 vol % Cr_3C_2 content composite is greater than for the 10 vol % Cr_3C_2 composite. These results are very different from the previous investigations [5, 8]; those results always showed a weight gain after oxidation if carbide-reinforced oxide matrix composites, because the oxidation of carbide-reinforced oxide matrix composites always loses carbon and gains oxygen, therefore the net weight change is a weight gain. The comparison of weight change between the two chemical reactions is adverse. Reaction 1 is a weight gain, but Reaction 2 is a weight loss.

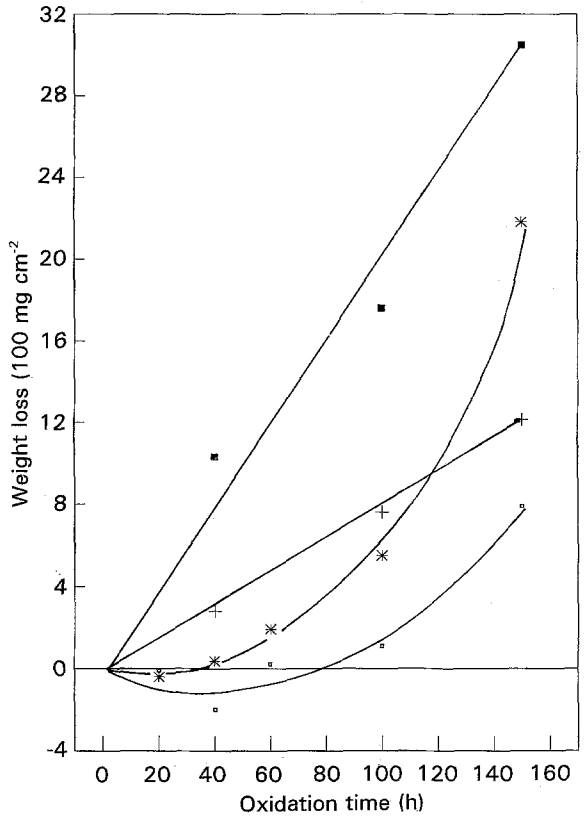

Figure 8 The weight change of (□, +) 10 and (*, ■) 30 vol % Cr_3C_2/Al_2O_3 composites with oxidation time at (□, *) 1000 °C and (+, ■) 1200 °C.

Let us make a quantitative analysis of the weight changes about the two possible chemical reactions. When a mole of Cr_3C_2 is oxidized, the weight gain of 48 g is much smaller than the weight loss, 300 g. So the weight change shown in Fig. 8 is initially weight gain and becomes a weight loss when the oxidation time exceeds 50 h at 1000 °C. Reaction 2 progresses more favourably when the temperature increases to 1200 °C [16]. So the weight loss directly occurs during oxidation of the composites, even when the oxidation time is very short, as shown in Fig. 8.

The scanning electron micrograph of a polished cross-section beneath the exposed surface of composites oxidized at 1000 and 1200 °C for 40 h is shown in Fig. 9. The normal microstructures of composites oxidized at 1000 and 1200 °C are observed in Fig. 9a and c, respectively. These are several black micropores within the oxidized layer and the white Cr_3C_2 particles are uniformly distributed in grey Al_2O_3 matrix. The chromium element's X-ray map corresponding to the micrographs of Fig. 9a and c are shown in Fig. 9b and d, respectively. The white spots of chromium enrichments are very consistent with Cr_3C_2 particles in the unreacted regions. With an oxidation temperature of 1200 °C for 40 h, the white spots are also uniformly distributed in the oxidized layer indicating

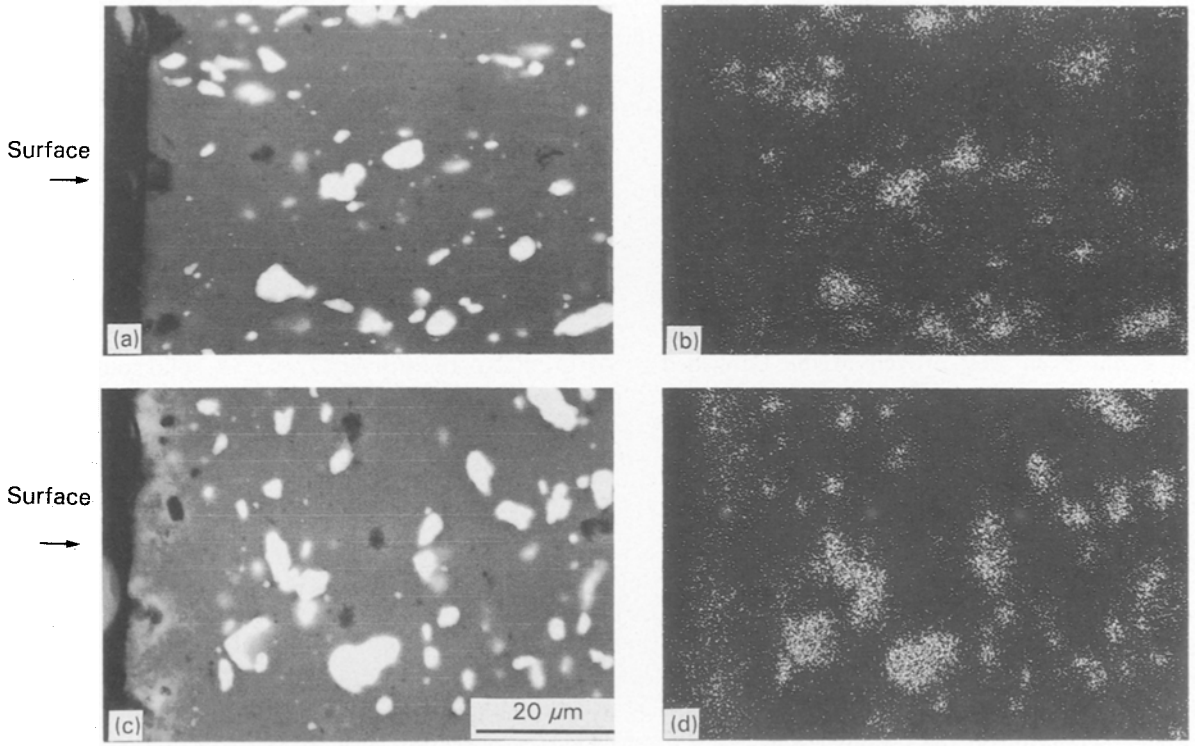

Figure 9 Cross-sectional scanning electron micrographs of 10 vol % Cr_3C_2/Al_2O_3 composites after oxidation at 1000 and 1200 °C for 40 h. (a), (c) Secondary electron images. (b), (d) EPMA, chromium element mapping. (a), (b) Oxidized at 1000 °C, (c), (d) oxidized at 1200 °C.

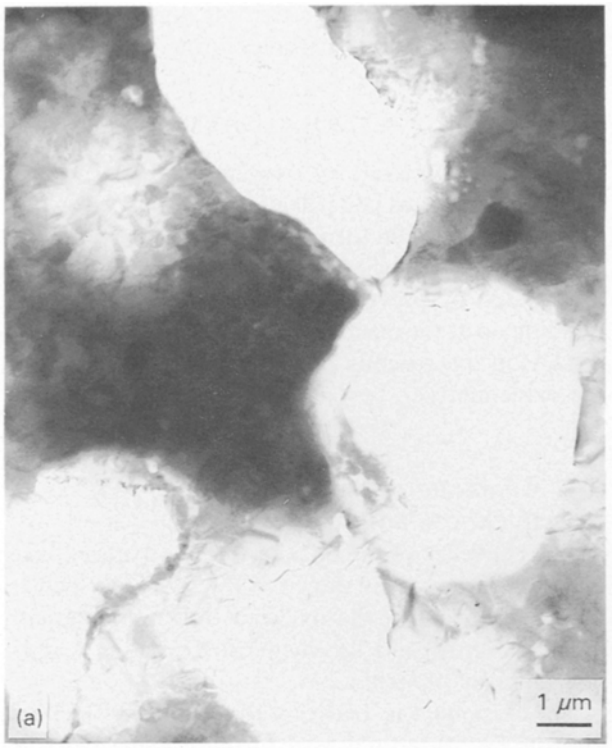

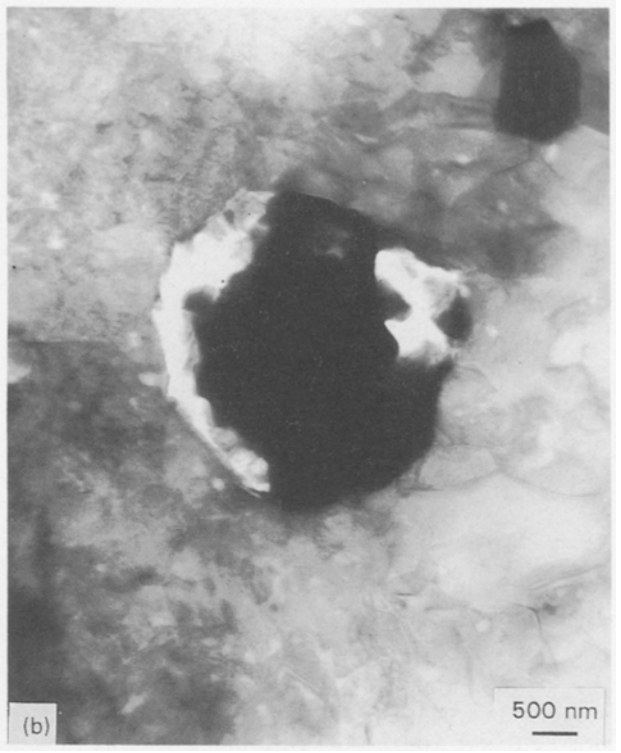

Figure 10 Transmission electron micrographs of 30 vol % Cr_3C_2/Al_2O_3 composites after oxidation at 1200 °C; (a) the oxidized layer, Cr_3C_2 completely oxidized to form micropores; (b) next to the oxidized layer, Cr_3C_2 partially oxidized; (c) the unoxidized region, Cr_3C_2 are black particles, Al_2O_3 matrix is grey. Microvoids and micropores are white.

that the product phase Cr_2O_3 dissolves to Al_2O_3 to form a solid solution shown in Fig. 9d, while there is no solid-solution formation in the oxidized layer shown in Fig. 9b, when the oxidation temperature falls to 1000 °C. These results are very consistent with the X-ray diffraction patterns observed in Fig. 7a and d. According to the phase diagram [20], both the constituents Cr_2O_3 and Al_2O_3 will form a complete solid solution. However, the Cr_2O_3 from the oxidized Cr_3C_2 with oxygen does not dissolve in Al_2O_3 at 1000 °C. The possible reason is that the kinetics of solid solution is very slow. When the oxidation temperature is increased to 1200 °C, the kinetics is enhanced rapidly and the solid solution may be obviously observed in Fig. 9d.

3.3. Microstructure

Typical transmitted electron micrographs of oxidized composites from the exposed surfaces to the unoxidized regions are shown in Fig. 10. There are several nodular spherical micropores in the Al_2O_3 matrix which are the typical microstructure beneath the exposed surface of the oxidized composites, shown in Fig. 10a. From the point of view of morphology and geometry, the white micropores are very similar to Cr_3C_2 particles. Next to the completely oxidized regions, white microvoids surround the black partially oxidized Cr_3C_2 particles, as shown in Fig. 10b. In the unoxidized region which is far away from the exposed surface of the oxidized composites, the Cr_3C_2 particles are still in their original shape, Cr_3C_2/Al_2O_3 interfaces are clean, and no micropores and microvoids are observed (Fig. 10c).

According to the previous microstructural observations, a schematic oxidation of Cr_3C_2 particles can be illustrated as in Fig. 11. Fig. 11a shows the unreacted region with Cr_3C_2 particles uniformly distributed in the Al_2O_3 matrix. Oxidation first takes place at the sample surface and proceeds inwards to the sample. As the reaction time increases, oxygen transport is driven by the oxygen potential gradient [21] across

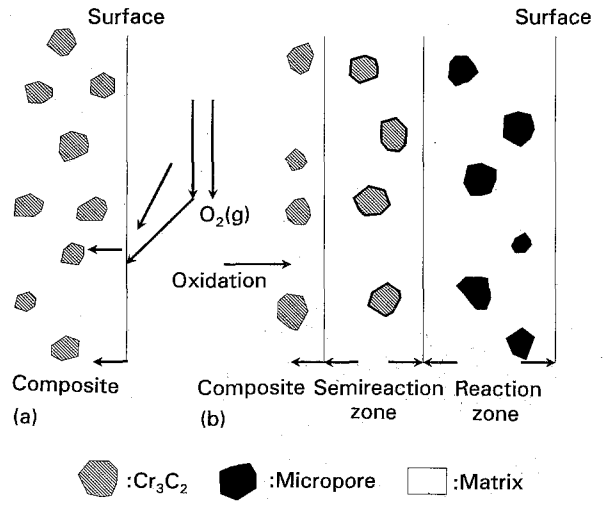

Figure 11 Schematic diagrams to illustrate the change of microstructure between (a) as-sintered and (b) oxidized composites.

the oxidized regions. As time passes, a completely-reacted zone, semireacted and unreacted zones can be differentiated under the electron microscope. If the oxygen diffusion in the oxide matrix is much faster than in the oxidized carbide product, all carbide particles will develop a reacted layer of finite thickness. On the other hand, if oxygen diffusion through the oxidation product is comparable to or faster than through the oxide matrix, the reaction product will be a phase mixture of the oxidation product and the unreacted matrix oxide [9, 21]. The above two cases represent two opposite extremes. An intermediate situation is possible, as shown in Fig. 11b. The interface between the reaction product and unreacted composites will not be sharp. There would be a region between reaction product and unreacted composites containing semireacted Cr_3C_2 particles.

The microvoids from the CrO_3 diffusing quickly outwards through the Al_2O_3 matrix. In the case where the Cr_3C_2 particle is completely oxidized and the CrO_3 is completely dissolved in Al_2O_3, the micropore forms at the site of the original Cr_3C_2 particle. Let us consider another gaseous product of CO. Much of the literature [6, 9, 13, 22] has reported that the permeability of CO gas in Al_2O_3 is much lower than that of oxygen in Al_2O_3. Therefore, the CO partial pressure will build up to be high enough to form large gas bubbles and fracture the oxide matrix into many pieces. This is the reason why a degradation of strength or toughness of carbide-reinforced oxide always occurs after oxidation treatment at high temperature. There are always flaws much larger than 50 μm observed in the micrograph of previously published papers [9, 13], larger in size than the critical flaw size (38 μm) of pure Al_2O_3 calculated by Griffith's law. In this experiment the reacted product Cr_2O_3 will further oxidize with oxygen to form CrO_3 gaseous product. In this case, the Cr_2O_3 plays a role of oxygen getter and the gaseous product CrO_3 will quickly dissolve in Al_2O_3. The concentration of oxygen at the Cr_3C_2/Al_2O_3 interface always retains a much lower value than that existing at the SiC/Al_2O_3 interface. Furthermore, we consider the following reaction to occur in which many carbides form gaseous compounds on oxidation

$$C_{(s)} + 1/2O_{2(g)} = CO_{(g)} \quad (3)$$

If the partial pressure of oxygen is low, the partial pressure of gaseous CO will also tend to drop towards the same value as in the gaseous phase. Therefore the detrimental effects of bubble formation or fracture can be avoided by preventing the oxygen pressure from building up at the reactant/oxide interface and quickly dissolving the gaseous product phase (like CrO_3) in the oxide matrix.

3.4. Characterization of oxidation thickness and reaction rate

The dependence of the thickness of the oxidized layer and exposure times is shown in Fig. 12. With increasing oxidation time, the oxidized thickness gradually grows inwardly and the chemical Reactions 1 and 2 continuously progress.

The correlations between the oxidized thickness and the exposure time varied from a linear equation for the shorter oxidation time to a square equation for the longer oxidation time. These results are very consistent with the linear-parabolic mode of Deal and Grove [18]. According to the linear-parabolic mode $[x^2 + Ax = B(t + \tau)]$, the linear and parabolic rate

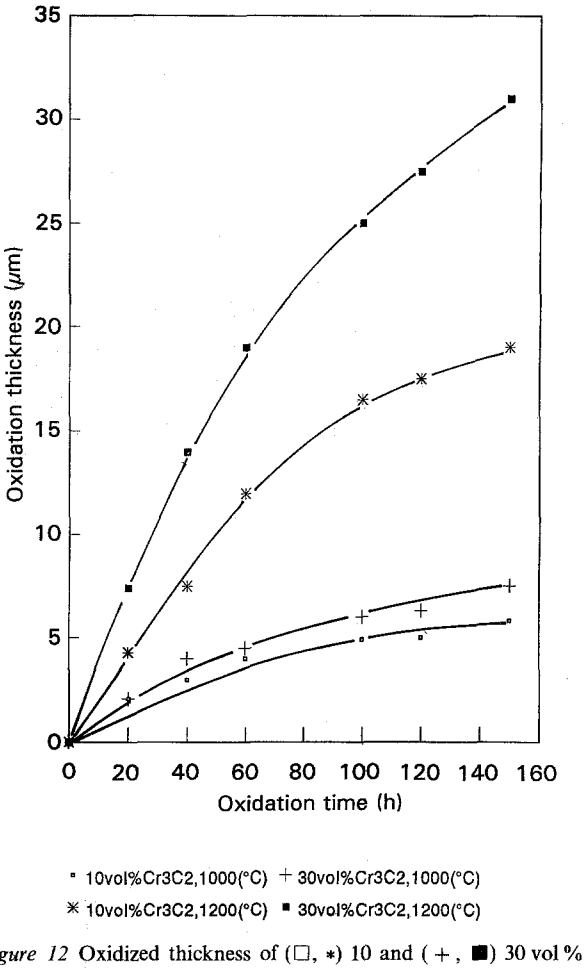

Figure 12 Oxidized thickness of (□, *) 10 and (+, ■) 30 vol % Cr_3C_2/Al_2O_3 composites with oxidation time at (□, +) 1000 and (*, ■) 1200 °C.

TABLE I The rate constant of oxidized Cr_3C_2-reinforced Al_2O_3 composites in air

Cr_3C_2 content (vol %)	Linear rate constant ($cm\,s^{-1}$)		Parabolic rate constant ($cm^2\,s^{-1}$)	
	1000 °C	1200 °C	1000 °C	1200 °C
10	1.9×10^{-9}	5.3×10^{-9}	5×10^{-13}	1.2×10^{-12}
30	3.1×10^{-9}	1×10^{-8}	1×10^{-12}	3.1×10^{-11}

particles will become great. According to Abderazzik *et al.*'s results [8], the diffusivity of oxygen in Al_2O_3 at 1000 °C is $2.6\times10^{-19}\,cm^2\,s^{-1}$. The diffusion zone $2(Dt)^{\frac{1}{2}}$ of oxygen in Al_2O_3 at 1000 °C for 100 h is 0.02 μm. This value is considerable lower than 4.2 μm which is the oxidation thickness of Cr_3C_2-reinforced Al_2O_3 composites oxidized under the same conditions. A previous paper [13] reports that the diffusion rate of oxygen through the oxide matrix with even

TABLE II Parabolic rate constant for the oxidation of monolithic ceramics or ceramic composites at 1200 °C

Material	Environment	Reference	Rate constant, K ($cm^2\,g^{-1}$)
30 vol % Cr_3C_2 Al_2O_3	Air	Present study	17×10^{-12}
30 vol % SiC_w/Al_2O_3	Air	Luthra *et al.* [13]	7×10^{-12}
36.7 vol %, SiC_w, 10.9 vol % ZrO_2/Al_2O_3	Air	Ricoult [24]	50×10^{-12}
SiC	Dry O_2 (g)	Costell *et al.* [2]	2.8×10^{-12}
Si	Dry O_2 (g)	Deal *et al.* [18]	1.3×10^{-12}

constants can be evaluated directly from Fig. 12 and are shown in Table I. The higher oxidized temperature and Cr_3C_2 contents, and the greater linear rate constants are given. This is an interface-controlled regime. The higher Cr_3C_2 content can provide greater opportunities to react with oxygen and the higher temperature can enhance the higher mobility of oxygen to reach the exposed surface. Thus the linear rate constants become greater. Similarly, the higher oxidized temperature and Cr_3C_2 content, and the greater parabolic rate constants are also given. This case is a diffusion-controlled regime. The higher Cr_3C_2 content can provide more vacancy concentrations originating from the micropores formed by the oxidation of Cr_3C_2 particles. A comparison of parabolic rate constants at 1200 °C between various monolithic and ceramic composite materials is shown in Table II. The rate constants of ceramic composites are always a hundred times higher than those of monolithic non-oxides. Because the ceramic composites invariably contain interfaces and microcracks which might be caused by thermal mismatch between reinforcement and matrix, the permeability of oxygen is greater than in the monolithic material. A passive film of SiO_2 will form at the interface of oxygen/silicon [18] or oxygen/silicon carbide [1, 2] to prevent the oxygen from further inward diffusion, because the permeability of oxygen in SiO_2 is very slow. Therefore the rate constants of silicon or silicon carbide are very low values. The diffusivity of oxygen [8] at 1000 °C, in ZrO_2 (about $3.0\times10^{-9}\,cm^2\,s^{-1}$) is much greater than that in Al_2O_3 (about $2.6\times10^{-9}\,cm^2\,s^{-1}$), because ZrO_2 has an oxygen vacancy as the predominant point defect and exhibits considerable non-stoichiometry compared to Al_2O_3. Although incorporating ZrO_2 particles in composites of SiC-reinforced Al_2O_3 matrix can double the toughening effects [23], the oxidation resistance drops by a great amount. So the parabolic rate constant of a composite containing ZrO_2 toughening extremely small cracks is much more rapid than through the densified oxide matrix without cracks. Owing to the many micropores existing in the oxidized layer of composites, the permeability of oxygen in the oxidized composites is higher than in fully dense Al_2O_3.

The greater the number of pores in the oxidized layer of a composite, the faster will be the diffusion rate of oxygen. So the oxidation rate of the composites increases with the Cr_3C_2 contents in the composites shown in Fig. 12. These results are very consistent with the previous study [9] in which the oxidation rate of SiC-reinforced Al_2O_3 composites was found to be proportional to the SiC content.

4. Conclusion

The oxidation treatment of Cr_3C_2 particle-reinforced Al_2O_3 composites has a strengthening and toughening effect on the composites at room temperature. In addition to the toughening mechanism of crack deflection, originally acting in the composites, crack blunting and energy dissipation are the primary toughening mechanisms arising from the micropores located beneath the exposed surface. During the oxidation of composites, two chemical reactions are involved. There are many micropores in the oxidized layer caused by the vaporization of gaseous CrO_3 phase. The oxidation behaviour follows the linear-parabolic mode. The oxidation rate is proportional to the Cr_3C_2 content in the composites and is more rapid than in the dense Al_2O_3 arising from the pores existing in the oxidized layer.

Acknowledgement

The authors thank the Ministry of Economic Affairs, Taiwan, for financial support under contract Mat. 3633220.

References

1. W. A. ZDANIEWSKI and H. P. KIRCHNER, *J. Am. Ceram. Soc.* **70** (1987) 548.
2. JOHN A. COSTELLO and RICHARD E. TRESSLER, *ibid.* **69** (1986) 674.
3. JOHN S. HAGGERTY and A. LIGFOOT, *ibid.* **72** (1989) 1675.
4. K. JAKUS, J. E. RITTER and W. P. ROGERS, *ibid.* **67** (1984) 471.
5. T. N. TIEGS and P. F. BECHER, *Ceram. Sci. Eng. Proc.* **7** [9–10] (1986) 1182.
6. E. E. HERMES and R. KERANS, in "Materials Stability and Environmental Degradation", edited by A. Barkatt, E. D. Verink, Jr and L. R. Smith, Materials Research Society Symposia, Proceedings Vol. 125 (1988) pp. 173–8.
7. M. P. BOROM, M. K. BRUM and L. E. SZALA, *Adv. Ceram. Mater.* **3** (1988) 491.
8. R. ARUN, M. SUBRAMANIAN and G. M. METHROTRA, in "Ceramic Transactions", Vol. 10, edited by Richard E. Tressler and Michanel, Mcnallan (American Ceramic Society, Westerville, OH, 1989) p. 211.
9. KRISHAN L. LUTHRA and HEE DONG PARK, *J. Am. Ceram. Soc.* **73** (1990) 1014.
10. C. T. FU, J. D. LIN and A. K. LI, presented at the 92nd Annual Meeting of the American Ceramic Society, Dallas, Texas, 22–26 April 1990, Ceramic Matrix Composites Symposium, Paper 84-SIV-90.
11. J. D. LIN, C. T. FU and A. K. LI, in "Proceedings of the 1991 Annual Conference of the Chinese Society for Materials Science", Taiwan, R.O.C., 26–28 April 1991, p. 640.
12. G. K. BANSAL, in "Proceedings of Eleventh National Symposium on Fracture Mechanics", Blacksburg, June 1978, edited by S. W. Freiman (NIST, Washington, 1978) pp. 38–46.
13. KRISHAN L. LUTHRA, in "Materials Stability and Environmental Degradation", edited by A. Barkatt, *et al.* Materials Research Society Proceedings, Vol. 125 (1988) pp. 183–95.
14. DIANE M. MLESKOWSKI, T. E. MITCHELL and A. H. HEUER, *J. Am. Ceram. Soc.* **67** [1] (1984) C17.
15. B. W. LIN and A. K. LI, in "Proceedings of the 1989 Annual Conference of the Chinese Society for Materials Science, Taiwan, R.O.C. April 1991, p. 696.
16. H. C. GRAHAM and H. H. DAVIS, *J. Am. Ceram. Soc.* **54** (1971) 89.
17. B. KUBOTA, *ibid.* **44** (1961) 239.
18. B. E. DEAL and A. S. GROVE, *J. Appl. Phys.* **36** (1965) 3770.
19. G. B. ABDERAZZIK, F. MILLIT, G. MOULIN and A. M. HUNTZ, *J. Am. Ceram. Soc.* **68** (1985) 307.
20. E. M. LEVIN, C. R. ROBBINS and H. F. MCMURDIE, in "Phase Diagrams for Ceramists". Edited by M. K. Reser (Am. Cera. Soc. Inc., Columbus, Ohio, 1979), p. 121.
21. C. C. LIN, A. ZANGHVIL and R. RUH, presented at the 91st Annual Meeting of the American Ceramic Society, Indianapolis, IN, 23–27 April 1989, Engineering Ceramics Division, Paper 7-JII-89.
22. T. A. RAMANARAYANAN, M. RAGHAVEN and R. PETKOVIC-LUTON, *J. Electrochem. Soc.* **131** (1985) 923.
23. P. F. BECHER, T. N. TIEGS, J. C. OGLE and W. H. WAREICK, in "Fracture Mechanics of Ceramics", Vol. 7 edited by R. C. Broat, A. G. Evans, D. P. H. Hasselman and F. F. Lange (Plenum Press, New York, 1986), p. 75.
24. M. B. RICCOULT, *J. Am. Ceram. Soc.* **74** (1991) 1793.

Received 5 January 1993
and accepted 29 April 1993